



Article

Complete Transitions of Hybrid Wind-Diesel Systems with Clutch and Flywheel-Based Energy Storage

José Luis Monroy-Morales ^{1,*} , Rafael Peña-Alzola ², David Campos-Gaona ³  and Olimpo Anaya-Lara ³

¹ Electrical Engineering, TecNM/Instituto Tecnológico de Morelia, Av. Tecnológico No. 1500, Morelia 58120, Mexico

² Electronic and Electrical Engineering, University of Strathclyde, 204 George St., Glasgow G1 1XW, UK

³ Wind Energy and Control Centre, Department of Electronic and Electrical Engineering, University of Strathclyde, 16 Richmond Street, Glasgow G1 1XQ, UK

* Correspondence: jose.mm@morelia.tecnm.mx; Tel.: +52-443-4641595

Abstract: A Wind Diesel Hybrid System (WDHS) is an isolated power system that combines Diesel Generators (DGs) and Wind Turbines (WTGs). The WDHS has three operation modes: Diesel Only (DO), Wind Diesel (WD) and Wind Only (WO). The latter mode is the only one resulting in substantial savings, as the DG consumes fuel even with no load. Moreover, adding an energy storage system (ESS) can significantly reduce the start/stop cycles in the DG. The FESS is robust, immune to deep discharges and its state of charge (SOC) is simple to monitor. The WDHS considered in this article uses a friction clutch to disengage the diesel engine (DE) from the synchronous generator (SG) in WO mode. The AVR regulates the voltage amplitude and the frequency regulation results from balancing the power produced by the DG and WT with the power consumed by the load and dump load along with the FESS utilisation. The control algorithms of the different elements present in the WHDS are explained, as well as the general control. The FESS always has priority over the DL for the maximum harnessing of the wind power. Simulations assess the proposed solutions for the different operation modes in the WDHS.



Citation: Monroy-Morales, J.L.; Peña-Alzola, R.; Campos-Gaona, D.; Anaya-Lara, O. Complete Transitions of Hybrid Wind-Diesel Systems with Clutch and Flywheel-Based Energy Storage. *Energies* **2022**, *15*, 7120. <https://doi.org/10.3390/en15197120>

Academic Editor: Adrian Ilinca

Received: 3 September 2022

Accepted: 26 September 2022

Published: 28 September 2022

Publisher's Note: MDPI stays neutral with regard to jurisdictional claims in published maps and institutional affiliations.



Copyright: © 2022 by the authors. Licensee MDPI, Basel, Switzerland. This article is an open access article distributed under the terms and conditions of the Creative Commons Attribution (CC BY) license (<https://creativecommons.org/licenses/by/4.0/>).

Keywords: isolated grid; flywheel energy storage; wind turbine; dump load; friction clutch

1. Introduction

A wind-diesel hybrid system (WDHS) is a combination of wind turbine generators (WTG) with diesel generators (DGs) used to provide electricity in areas without connection to the main grid. The WDHS can work in the following operation modes: Diesel Only (DO), Wind Diesel (WD), and Wind Only (WO) [1]. The DO mode occurs when the wind speed is insufficient and the DG provides the active and reactive power required by the consumer load. In WD mode, the wind speed is sufficient and the WTG starts producing power. This reduces the amount of power supplied by the DG and the WTGs can be regarded as negative loads. In DO and WD modes, the speed governor of the diesel engine (DE) regulates the system frequency and the automatic voltage regulator (AVR) of the synchronous generator (SG) regulates the voltage amplitude.

The WD mode does not result in a substantial reduction in fuel consumption and emissions. This happens because of the Willans curve, which shows that the DE consumes fuel even with no load (up to 40%, [2]). Hence, the DE should be shut off so that the wind resource achieves the highest contribution to the total produced power. In WO mode, the WTGs can generate a surplus of active power during periods of high wind speed. Consequently, additional components are needed to balance the generated and consumed active power. Controllable loads are used to counteract the power excess, typically dump loads (DL). The DL simply dumps the power excess into resistors; the resulting energy dissipation is used for heating the DE itself. Moreover, the addition of an energy storage system (ESS) allows reducing significantly the number of start/stop cycles in the DG. The

ESS can store the wind power excess and can supply power during periods of low wind speed [3] as long as it is fully discharged. The DL is always necessary for the case when the ESS is fully charged and cannot store more energy.

There are many types of ESS such as batteries, superconducting magnetic energy storage systems (SMESs), super-capacitors (SC), and flywheel energy storage systems (FESSs) [4–6]. Many applications use batteries, in particular Li-ion, because of their high energy density at a constantly reducing cost. The lifetime depends on ambient temperature and the number of charge/discharge times [7]. Additionally, batteries have a limited rapid charge/discharge rate and sometimes the depth of discharge (DOD) is limited at the expense of longer lifetime [8].

Flywheel energy storage systems (FESSs) have been developed rapidly with the advance in power electronics, electrical machine technology, new materials, and magnetic suspension technology in the last thirty years [9]. The FESS technology has significant advantages such as: high reliability, high efficiency and fast dynamics [10,11]. FESSs allow the exchange of high power in a short time and the state of charge (SOC) is accurately estimated by just measuring the flywheel speed. FESSs are less affected by temperature when compared to other ESSs. FESSs result in long service life with low maintenance cost [12] and environmentally friendly disposal [5,13,14]. The FESSs are used in applications such as: the fluctuation suppression of renewable-based generating systems, uninterruptible power system (UPS), voltage and frequency control [6,15], energy recovery for railway applications [16–18] and isolated grids [19–21]. The rotor of the electrical machine is coupled to the flywheel [22], which can act as a motor to accelerate or as a generator to decelerate [23]. Power electronic converters enable the bidirectional power flow between the isolated grid and the FESS with a fast response.

In [24], the study of a wind-diesel system using superconducting magnetic energy storage is presented. The proposed system uses multiple WTGs, two DGs, and two SGs, which increases the system cost. Moreover, the active and reactive power controllers for the system are based on fuzzy logic, representing greater complexity due to the multiple machines that must be controlled. The dynamics of a small autonomous wind-diesel system are investigated in [25]. It defines the factors involving the system behaviour such as the speed governor and pitch controller. The system operates without an energy storage system, leading to difficulties in achieving a balance between the supplied and demanded power. In reference [26], the analysis of a hybrid power system consisting of wind turbines, diesel generators, a water pump as a secondary load, and a local load is presented. The proposed system does not include an energy storage system which implies the disadvantages mentioned above. The reference [27] presents a comparison between a constant speed flywheel, a variable speed one based on a power electronic converter, and a variable speed flywheel with hydrostatic transmission. In [28], a flywheel energy storage system is connected to a wind turbine and a constant voltage source. The main aim of this investigation is to regulate the system frequency. The wind turbine features are not clearly described and the power electronics converters are not described in detail. Research has also been carried out combining flywheels with other types of generation sources. In [29], a system combining a PV system and a diesel generator is presented which includes a flywheel-based energy storage system. For the simulation results, it is assumed that the PV array can constantly provide power to supply an average demand load. The system does not incorporate a clutch to disengage the diesel generator.

This paper presents the design and simulation of a WDHS, which is conformed by a DG, WTG, FESS, DL, and a consumer load as illustrated in Figure 1. The proposed system can operate in all the three operation modes of a WDHS: DO, WD and WO. The operation modes are determined by the wind availability and can be enabled/disabled via a friction clutch. The FESS and the DL are used as controllable loads to store/consume the excess power. The FESS is used as a controllable source to offset the power deficit. An appropriate controller for power sharing between the FESS and DL is developed. The controller takes into account the SOC (flywheel speed) of the FESS. In the case of high wind speed, the

FESS consumes excess active power if the SOC is below 95%. It is considered that the FESS can no longer store energy when the SOC reaches 95% and the DL consumes the active power excess. During periods of low wind speed, the WT can not supply the active power required by the consumer load and the FESS supplies the stored energy to the consumer load. If the low wind persists and the FESS energy is exhausted, the friction clutch activates the DG to supply active power to the consumer load.

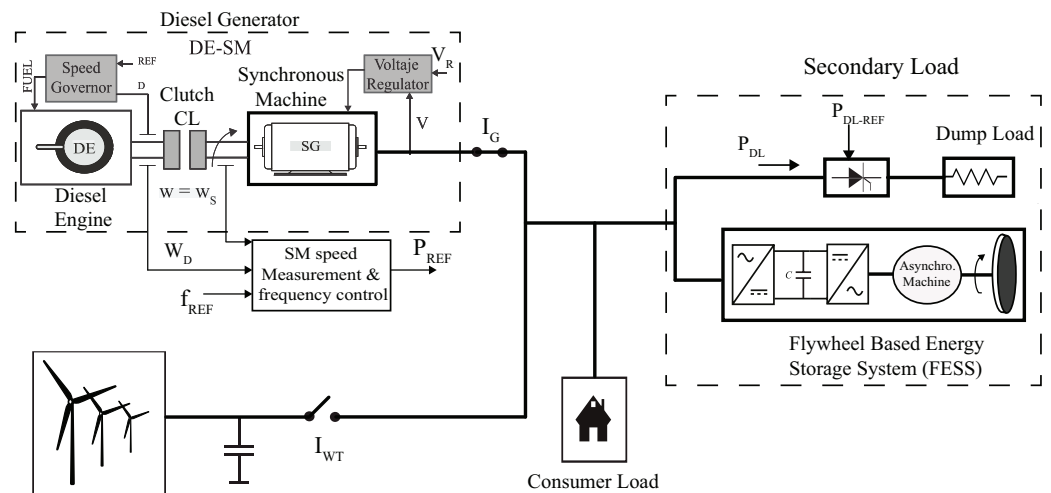


Figure 1. Wind-Diesel Power System.

This paper is organised as follows: Section 1 presents the modelling of the different elements in the WDHS. Section 2 explains the control of the WDHS control for the three operation modes. Section 3 presents the simulation results for different study cases. Finally, the conclusions of the paper are described in Section 4.

2. Wind Diesel Power System

The components conforming to the WDPS are shown in Figure 1. The consumption or generation of active power can be controlled or not depending on each element. The WT supplies uncontrollable active power because of the dependence on wind speed, which is random in nature. The consumer load absorbs uncontrollable active power and depends on the habits of the dwellers. The DG provides active power controlled by the speed regulator. The DL absorbs active power in a controlled manner by varying a binary sequence of resistor connections. The FESS is a mechanical battery which can absorb or supply controlled active power at will as ordered by the appropriate controller. Both, the DL and FESS are working as secondary loads. The reactive power is controlled in the DG through the automatic voltage regulator (AVR); the reactive power consumed by the WT is compensated by using a capacitor bank.

The Diesel Engine (DE) is connected to a synchronous machine (SM) by using a friction clutch as shown in Figure 1. The clutch is used to engage and disengage the DE to the SM so that the DG supplies active power when the clutch is engaged. The switch I_{WT} is closed for WD and WO modes and is opened for DO mode. Therefore, wind availability determines the operation states of the clutch and the I_{WT} switch, which defines the operation modes of the WDPS.

When the clutch is disengaged, the SM operates with no prime mover as a synchronous condenser and provides the voltage waveform in the WDPS at all operation modes. Therefore, the switch I_G next to the SM is permanently closed ($I_G = ON$).

The DO operation mode occurs when the clutch is engaged ($CL = ON$) and the switch I_{WT} is open ($I_{WT} = OFF$). The full active power is provided by the DG with no wind power involved. With the clutch engaged and as soon as the cut-in speed is reached, the switch I_T is closed ($I_T = ON$) and the WT starts producing power leading to the WD mode operation. In WO operation mode, there is sufficient wind power to supply the

load, the clutch is disengaged (CL = OFF) so that no power is provided by the DE. For this case, the SM still provides the voltage waveform and the reactive power working as a synchronous condenser.

2.1. Diesel Generator

The DE converts the fuel energy into mechanical power P_{MEC} at the shaft through the combustion process. In turn, the SM converts the mechanical power into electrical power. The rated power and inertia constant of the SM are 300 kVA and 1 s, respectively. The SM speed governor located in the DG regulates the system frequency, which is the SM speed times the number of pole pairs. The speed regulator uses a PID controller where the input is the speed error and the output is the fuel rate. The AVR regulates the voltage amplitude in the isolated network. The AVR varies the excitation current in the SM so that the voltage amplitude is within the prescribed limits.

The utilisation of a clutch allows using a single SM as a generator and a synchronous condenser. The clutch disengages the DE from the SM during the WO operation mode. In the overall controller, the state of the clutch is determined by a binary input signal. As long as the input signal is high, the clutch applies a normal force through a pressure actuator. The static friction prevents the surfaces from slipping and torque transmission is possible. When the binary signal is zero, the pressure actuator is released, the clutch surfaces are separated and no torque is applied to the SM. The clutch modelling using the Simscape library of Matlab/Simulink is shown in Figure 2.

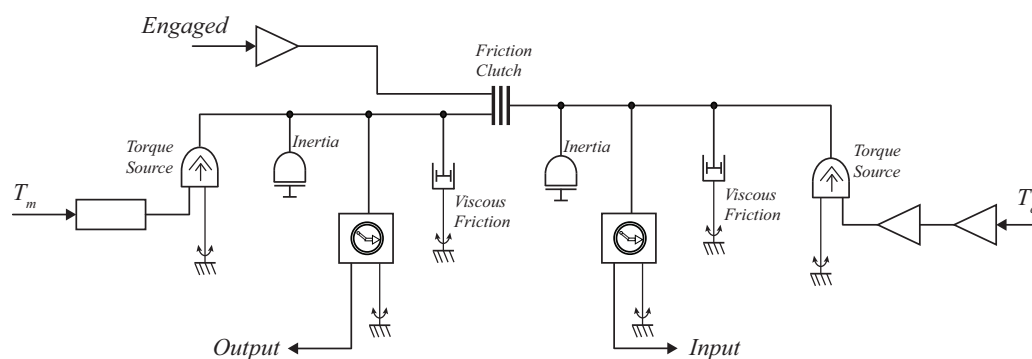


Figure 2. Clutch.

2.2. Wind Turbine

The fixed-speed wind turbine is rated 275 KVA and is connected to a Squirrel-Cage Induction Generator (SCIG) through a gearbox. The WT transforms the wind power into mechanical power at the shaft. In turn, the SCIG is directly coupled to the grid and transforms the mechanical power into electrical power. To correct the power factor, a 25 kVA capacitor bank is placed at the WTG-SCIG terminals as shown in Figure 1.

The fixed-pitch WT uses a lookup table that relates the WT shaft speed ωt with the mechanical power at the shaft P_{T-MEC} . The SCIG presents only small variations in the speed constant speed generator between 1 and 1.02 per unit [30]. Thus, this type of turbine does not allow variations in the rotational speed in order to maximise wind power capture. For isolated systems, the fixed-pitch WT-SCIG represents an appropriate option because of its robust construction and simple maintenance. Moreover, the WTG-SCIG can provide additional damping to the system frequency since the wind power is proportional to the slip [31].

2.3. Dump Load

The DL is a secondary load consuming the active power excess produced by the WTG to balance the overall WDPS active power. Moreover, the DL is also a safety element necessary to prevent the reverse power in the DG in operation mode WD. With reverse power, the DG is consuming power instead of producing it; this represents a potentially

dangerous situation. Hence, the WDPS must order to connect the dumping load so that the DG always supplies a minimum load.

The DL consists of three-phase binary resistors connected in parallel.

$$R, \frac{R}{2}, \frac{R}{2^2}, \frac{R}{2^3} \dots \frac{R}{2^7} \quad (1)$$

The resistors are connected to the grid using a zero-crossing thyristor with no harmonic injection. The largest resistor R consumes the following power P_0 :

$$P_0 = \frac{V_s^2}{R} \quad (2)$$

where V_s is the rated voltage of the system. The rated power of the resistors can be calculated as a binary sequence multiplied by P_0 , as follows:

$$2^0 P_0, 2^1 P_0, 2^2 P_0, 2^3 P_0 \dots 2^7 P_0 \quad (3)$$

When considering the connection of the different binary resistors, the total power consumed by the DL, P_{DL} , is calculated as:

$$P_{DL} = (2^0 \cdot S_0 + 2^1 \cdot S_1 + \dots + 2^7 \cdot S_7) \cdot P_0 \quad (4)$$

where S_n is the switch state with $n = 0 \dots 7$ for the three phases. The P_{DL} value can be varied in discrete steps from 0 to $255P_0$. The base power P_0 for the DL is selected to be 1.75 kW and the maximum power P_{D-NOM} corresponds to 446.25 kW (1.75 kW \times 255).

2.4. Model for the Flywheel Energy Storage System

A flywheel stores energy mechanically in the form of kinetic energy. The kinetic energy is converted into electrical energy using an electrical machine, which can operate as a generator/motor. The kinetic energy stored is given by:

$$E_k = \frac{1}{2} I (\omega_{r-max}^2 - \omega_{r-min}^2) \quad [J] \quad (5)$$

where I is the moment of inertia and the ω_{r-max} and ω_{r-min} are the maximum and minimum angular velocity, respectively. The moment of inertia is determined by the mass and geometry of the flywheel and is defined as:

$$I = \int d^2 dm_d \quad [\text{kg} \cdot \text{m}^2] \quad (6)$$

where d is the distance from the axis of rotation to the differential mass dm_d .

The development of high-strength composite materials (carbon fibres combined with epoxy resin) allows the construction of high-speed flywheels. The material is very light but because the energy stored in the flywheel depends on the rotation speed, they result in flywheels with elevated energy density. The utilisation of magnetic bearings and vacuum containment minimises friction losses. On the other hand, inexpensive and reliable steel flywheels allow achieving an elevated moment of inertia due to the high density with medium rotation speeds.

In an EES for an isolated hybrid wind-diesel system, space requirements are not stringent, the amount of energy required for a substantial reduction in the number of start/stop cycles is in the order of minutes of the average load and the round trip efficiency does not have a substantial impact [32]. Hence, a steel flywheel is selected due to cost and easy maintenance considerations [33].

The selected machine for driving the flywheel is a permanent magnet synchronous machine (PMSM) because of its high efficiency. For interfacing the FESS with the isolated grid, a two-level back-to-back three-phase converter is used as illustrated in Figure 3.

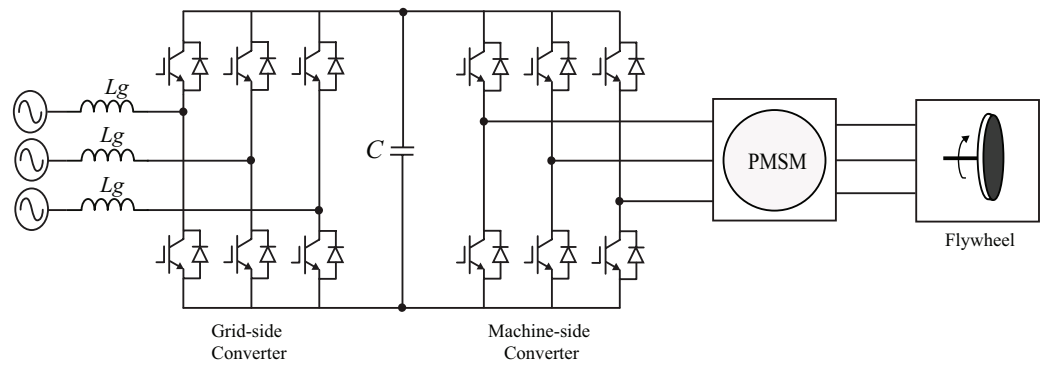


Figure 3. Power Converters in a FESS.

In Figure 3, the grid-side converter regulates the DC voltage, which determines the active power exchanged by the FESS. The reactive power reference in the grid-side converter is set to zero for the unity power factor leading to maximum efficiency. The inductor L_g is used to limit the harmonic content injected into the grid due to the PWM commutations. The controller implementation for the grid-side converter is as shown in Figure 4. It uses voltage-oriented control synchronised to the grid by using a phase-locked loop (PLL) with inner current loops. There is a feed-forward component in the DC-voltage control with the power reference for faster dynamic response.

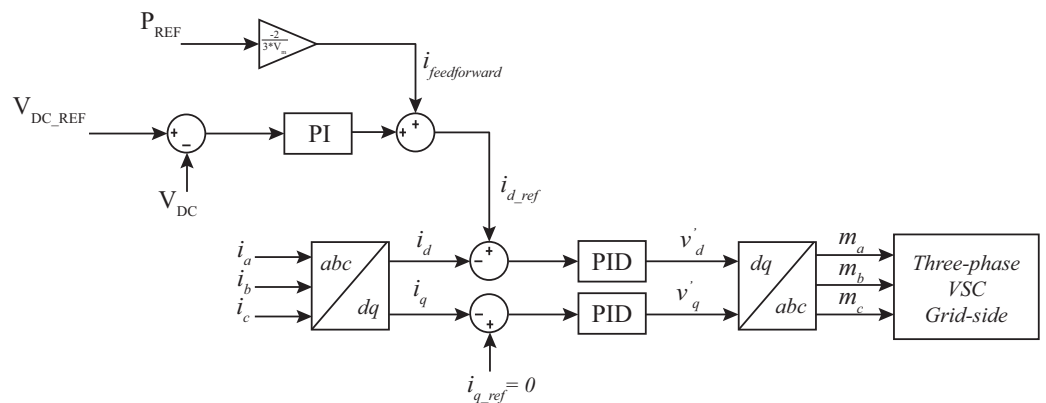


Figure 4. Grid-side controller.

Field-Oriented Control (FOC) is a well-known technique to control the PMSM. FOC allows having control capacity over the full speed with current protection. In speed control mode, the motor controller generates the torque reference necessary so that the speed reference is followed. The torque reference is proportional to the dq -currents that are limited by the motor controller. The stator currents are transformed from the stationary reference frame ($\alpha - \beta$) to the rotor flux reference frame ($d-q$). The flux equations for the PMSM are as follows:

$$\psi_d = L_d i_d + \psi_p \tag{7}$$

$$\psi_q = L_q i_q \tag{8}$$

where ψ_d and ψ_q are the flux linkage of the direct and quadrature axis of the PMSM, respectively. L_d and L_q are the direct and quadrature inductance, i_d and i_q are the direct and quadrature currents and ψ_p is the permanent magnet flux linkage. The equation for torque calculation is:

$$T = p(\psi_p i_q + (L_d - L_q) i_q i_d) \tag{9}$$

where p is the number of pole pairs. In Equation (9), a factor of $3/2$ must be considered, since the power of the three-phase system is represented in a two-axes orthogonal sys-

tem. For the PMSM with surface mount magnets $L_d = L_q$ and the Equation (9) can be rewritten as:

$$T = \frac{3}{2} p (\psi_p i_q) \quad (10)$$

Neglecting the losses in the stator iron and stator and rotor resistance, the PMSM active power exchanged is the product of the electromagnetic torque T_e and the PMSM rotor speed ω_m . In addition, if the FESS back-to-back converter losses are neglected, the active power exchanged between the FESS and the isolated grid P_{fs} is approximately calculated as:

$$P_{fs} = T_e \omega_m \quad (11)$$

Considering the electrical dynamics, the speed ω_r is approximately constant because the flywheel has high inertia. Therefore, the i_q regulates the FESS exchanged power using a required reference value. In this paper, the flywheel speed range is between $\omega_{r-min} = 1500$ rpm and $\omega_{r-max} = 3300$ rpm, and the FESS rated power (P_{S-NOM}) is 150 kW. The FESS-rated power should be supplied during 2 min [12], the period where the wind turbulence is located in the power spectrum.

The PMSM-rated power is 300 kW, 60 Hz, with 2 pole pairs so that it can provide the FESS-rated power at half speed. The PMSM model uses a block included in the SimPowerSystems library of Matlab/Simulink. The controller for the grid-side converter is shown in Figure 4 whereas that of the machine-side converter is as shown in Figure 5.

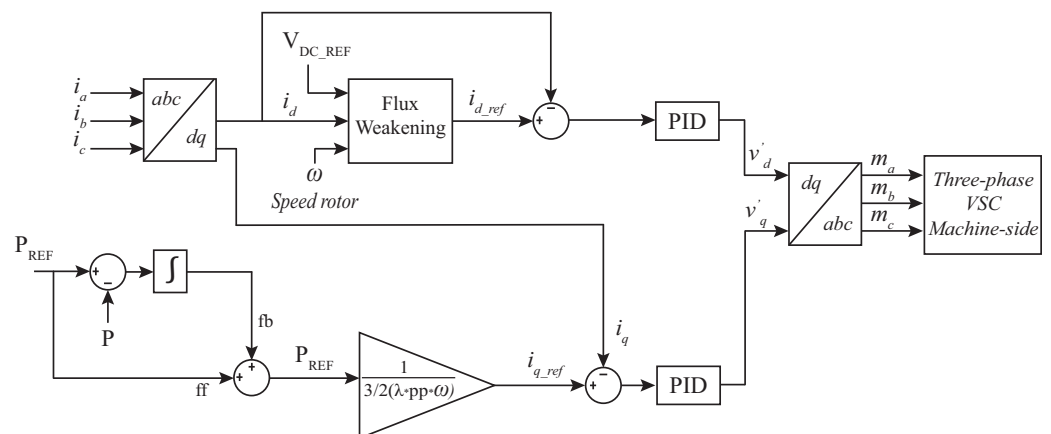


Figure 5. Machine-side controller.

The grid-side converter uses voltage vector-oriented control, which is analogous to field-oriented control. Using a PLL, the d-axis is aligned to the grid voltage vector. The inner control loops correspond to the dq-current. The outer control loop corresponds to the DC-link voltage and sets the d-current reference. The q-current reference is set to zero for achieving the unity power factor. There is a feed-forward component in the d-current reference corresponding to the power exchanged as expressed in (11). The machine-side converter used field-oriented control; the d-reference is set to zero for achieving the maximum torque per stator current. The q-reference also has the previous feed-forward component as expressed in (11) for setting the power exchanged between the FESS and AC grid. In order to correct steady-state errors, there is a closed-loop component resulting from integrating the error between the power reference and power exchanged between the FESS and the grid.

3. Control of the WDPS

An appropriate control for the clutch must be designed since it is a crucial element when selecting a required operation mode. The locking of the frictional clutch results in the engagement of the DE and SM for the DO and WD operation modes, causing the DE speed governor to control the system frequency. The frequency regulation is achieved by

balancing the produced and consumed active power in the isolated system. The power equation of the SM during WD operation mode is as follows:

$$P_{DE} + P_{WTG} - P_{CL} - \underbrace{P_{FESS} - P_{DL}}_{\text{Controllable Loads}} = J\omega \frac{d\omega}{dt} \quad (12)$$

where P_{DE} is the active power supplied by the DE, P_{WTG} is the power supplied by the WTG, P_{CL} is the power consumed by the load, P_{FESS} is the power supplied or absorbed by the FESS, P_{DL} is the power consumed by the DL, J is the SM inertia and ω the SM shaft speed. The active power of P_{DE} and P_{WTG} are considered positive when generating and the active power of P_{DL} and P_{FESS} are considered positive when consuming. In a steady state and with proper regulation, the derivative of (12) is zero with the frequency constant and equal to the rated value.

For achieving a proper speed regulation, the diesel speed governor must be capable to order the required power P_{DE} to match with the resulting balance of active power expressed in Equation (12).

Assuming that FESS and DL are not operating, Equation (12) is as follows:

$$P_{DE} + P_{WTG} - P_{CL} = 0 \quad (13)$$

Thus, P_{DE} is:

$$P_{DE} = P_{CL} - P_{WTG} \quad (14)$$

From (14), if the power of the WTG (P_{WTG}) is higher than the power consumed by the consumer (P_{CL}), the power of the DE is negative and the DG is no longer capable to achieve frequency control and for this reasons, controllable loads are necessary. The power P_{DE} becomes positive when FESS absorbs active power and DL consumes active power so that the speed governor can regulate the frequency. If $P_{CL} - P_{WTG}$ persists in increasing beyond the capacity of the controllable load, the WTG should be disconnected by opening the I_{WT} switch. For WDHS with high penetration, the system control must order disconnect the SG from the DE by disengaging the clutch in order to change to WO operation mode. In WO operation mode, the WTG is capable of supplying all the necessary power to the consumers and this mode results in substantial savings in fuel consumption.

4. Control for Wind-Only Mode

In the WO operation mode, the WTP is the only power source present as the SM is disengaged from the DE. The powers P_{CL} and P_{WTG} are random depending on consumer habits and wind speed, respectively. Hence, the FESS and the DL are necessary to carry out the active power balance so that speed regulation is possible in the SG working as a synchronous condenser.

In WO mode, the SOC of the FESS is an important variable since it determines the capability to supply or absorb active power. Measuring the SOC of the FESS is very simple, unlike the case of the batteries, as it just requires measuring the flywheel speed. In order to use all the energy storage capability, a power-sharing algorithm between the FESS and DL is used taking into account the SOC of the FESS.

In Figure 6, the SOC of the FESS operates at a maximum of 95% and a minimum of 45%. The battery is considered completely charged when $\text{SOC} > 95\%$ and can not absorb wind power excess, but it can provide active power to the consumer load. The mechanical battery is considered discharged when $\text{SOC} < 45\%$; it can not provide power to the consumer load, but it can consume the wind power excess. The mechanical battery can exchange the rated power for both directions ($\pm P_{FESS_nom}$) when $45\% < \text{SOC} < 95\%$.

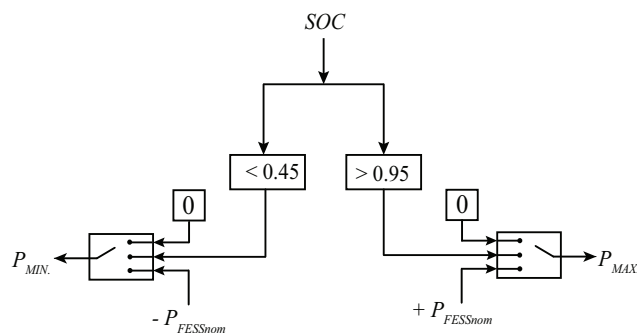


Figure 6. Maximum and minimum controllable power according to the Flywheel SOC.

A PI controller is used to regulate the frequency in WO mode. Figure 7 shows the transfer function relating to the controllable power P_C (P_{FESS} and/or P_{DL}) and the SM speed ω . This figure considers (12) with $P_{DE} = 0$ (WO mode).

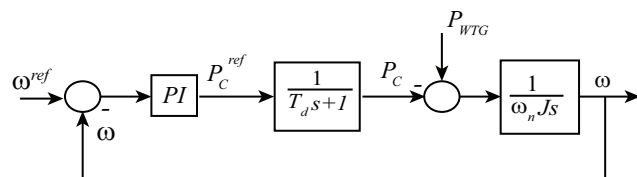


Figure 7. Frequency control with the synchronous condenser.

In Figure 7, the closed-loop control cancels the power P_{WTG} since it is considered a disturbance. The speed error is the input for the PI controller and the output of the PI controller is the power that the DL and/or the FESS takes as a reference.

The power P_C is not established instantaneously but takes a delay T_d determined by the voltage zero-crossing needed to connect the binary resistors or dynamic response of the current loop in the power converter. This delay is much shorter for the FESS case because it uses a pulse-width modulation (PWM) power converter.

The frequency is not calculated from the SM speed sensor but estimated from the three-phase grid voltage by using a PLL. This is analogous to sensorless speed estimation in motor control [34] and simulations show that the dynamic response is sufficiently fast because of the large SG inertia. The output limits of the PI controller for anti-windup consider the power limits of the DL and FESS (as long as its availability is based on the SOC) as per Figure 8.

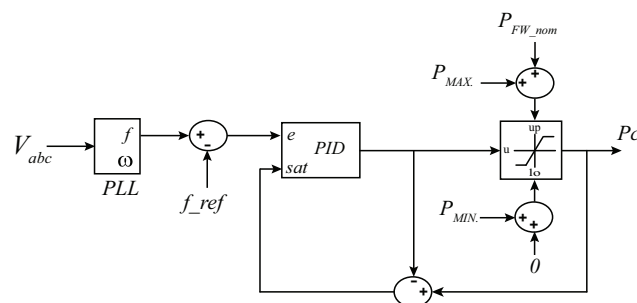


Figure 8. PI regulator for frequency control.

The plant of the frequency control follows (12) and is a simple integrator. A proper PI tuning procedure for this plant is a symmetrical optimum criterion [35]. The proportional gain and the integration time should be adjusted as follows:

$$K_p = \frac{\omega_n J}{a T_d} \tag{15a}$$

$$T_i = a^2 T_d \quad (15b)$$

with $a = 3$ for triple-pole response [36] and ω_n the rated frequency in radians per second. The output power reference of the PI controller, shown in Figure 8 is shared between the DL and the FESS. The delay T_d considered in the PI tuning corresponds to the binary resistors. It consists of the period required to connect the three-phase binary resistors in the zero-crossing, which accounts for a half cycle. However, simulations resulted in oscillations for this value because of the relatively small inertia constant and three times this value was used for properly damped waveforms.

In the power-sharing algorithm shown in Figure 9, the FESS has priority over the DL in order to store the maximum energy in the periods of wind power surplus. The load-sharing algorithm considers the discrete nature of the binary resistors (with steps of 1.75 kW for this case). The reference power to the DL is rounded in order to obtain multiples of the power step with the fractional part being directed to the FESS reference power.

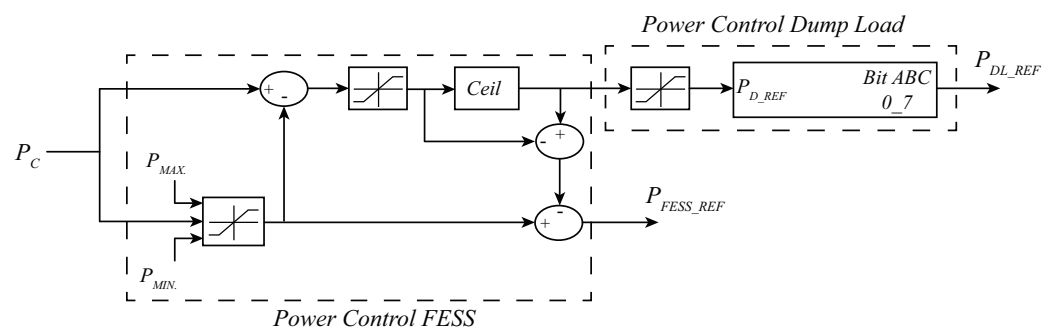


Figure 9. Power-Sharing control algorithm between the FESS and the DL.

When the SOC reaches 95%, the DL starts consuming the power excess that the FESS can no longer store. The frequency regulation presents no stability issues because the PI gains were selected for the DL case. When the SOC becomes lower than 45%, the FESS is considered to be discharged (as it could not provide full power). Thus, the frequency will decrease and the complete control should command the DG to begin providing power to avoid the system collapse by changing to the WD operation mode.

5. Simulations Results

Simulations of the WDHS represented in Figure 1 were carried out in order to demonstrate the validity of the proposals with different case studies being considered. The parameters used for simulations are as follow: the SM power is 300 kVA, 275 kVA WT, a 150 kW FESS and a 446.25 kW DL (255 steps of 1.75 kW each).

The first case study evaluates the WDHS only in WO operation mode. In this case, the DG is not operative and the WT provides the required active power to the consumer load. The surplus of active power produced by the WT is stored by FESS and/or dissipated by the DL, with the FESS having the maximum priority and taking into account the SOC. The second case study simulates the WDHS initially operating in WO mode with a decrease in wind speed that leads to a change in the operation mode to DO. During the period of low wind speed, the DG provides the active power needed by the consumer load. Finally, the third case study considers an initial low wind speed with the DG generating the required active power. Later, the wind speed increases and the system must change to WO operation mode by disengaging the DG.

5.1. Case Study 1

In this case, the WDHS operates in WO mode, the WT provides the active power required by the consumer load and the active power excess is consumed by the secondary loads, FESS and DL. The SOC is at 50% so that the FESS can store the power when required.

Figure 10 shows the active power generated by the WTG for different wind speeds. The WTG generates 340 kW for a wind speed of 12 m/s, 270 kW for 11 m/s and 200 kW for 10 m/s. The consumer load is initially 85 kW, decreases to 35 kW for a period, and increases again to 85 kW.

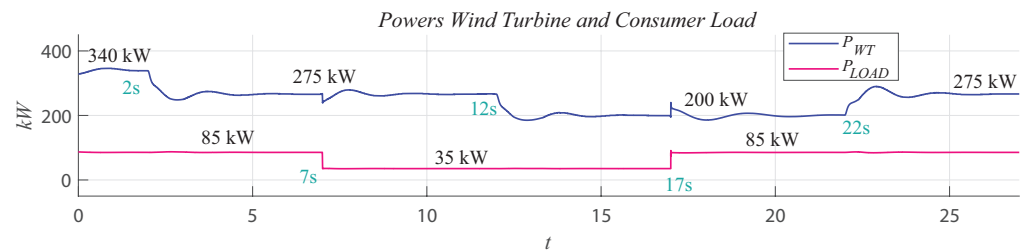


Figure 10. Power wind and consumer load for case study 1.

In the period from $t = 0$ s to $t = 2$ s, as illustrated in Figure 10, the P_{WTG} supplies 342 kW and the load consumes 85 kW, meaning that there is a surplus of active power. The FESS absorbs 150 kW (its full rated power) of the active power excess as can be seen in Figure 11. Because the FESS cannot absorb all the excess active power, the DL must consume the rest of the active power excess as shown in Figure 12 corresponding to 104 kW. Consequently, the active power consumed by the load, stored in the FESS, or dissipated by the DL and additional losses is matched with the active power generated by the WTG during this period.

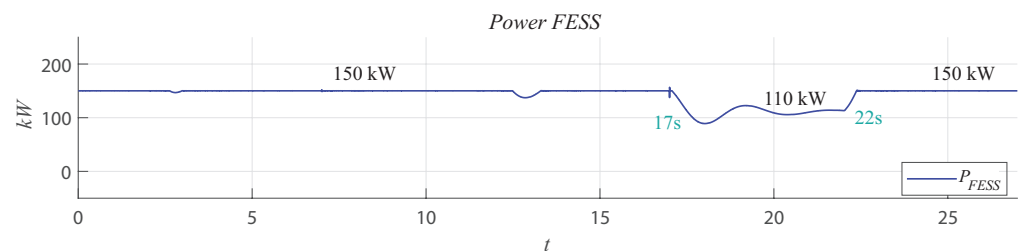


Figure 11. Power absorbed by the FESS for case study 1.

In the same Figure 10, the load consumption decreases to 35 kW at $t = 7$ s and the WTG supplies only 275 kW because the wind speed decreased; the active power excess persists but in a lesser amount. In this case, the FESS still absorbs the full power of 150 kW, but the DL consumption decreases to 87 kW for matching the wind power production.

It can be seen that the power-sharing algorithm gives priority to the FESS over the DL when dealing with the wind power excess in WO mode. Figure 11 shows a reduction in the power absorbed by the FESS down to 110 kW, from $t = 17$ s to $t = 22$ s, because of a decrement in the wind power excess when the wind speed decreases and the consumer load increases. In the same period, as Figure 12 shows, the DL stops consuming active power because there is no longer sufficient wind power excess and only the FESS deals with the surplus.

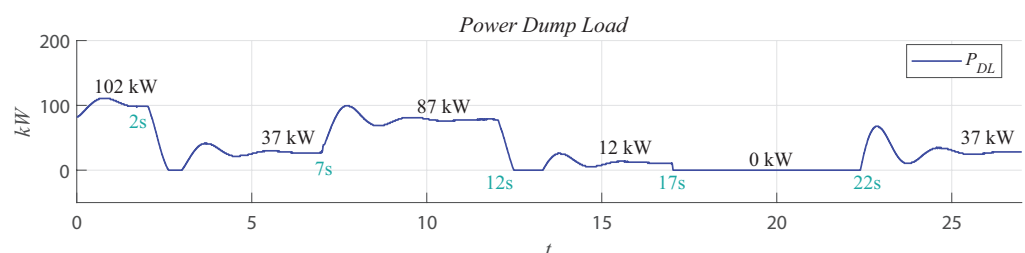


Figure 12. Power in the DL for case study 1.

The SG is working as a synchronous condenser with no power generation; it consumes a minimum active power, which corresponds to the mechanical losses, as can be seen in Figure 13.

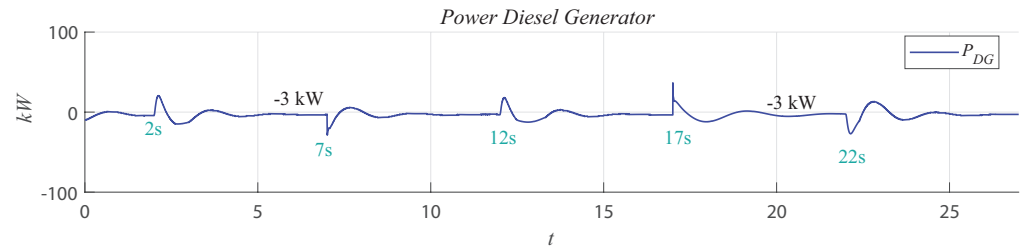


Figure 13. Power in the DG for case study 1.

Figure 14 shows the system frequency variations in the per unit system. These variations are appropriately damped when changes in the wind speed and the consumer loads take place.

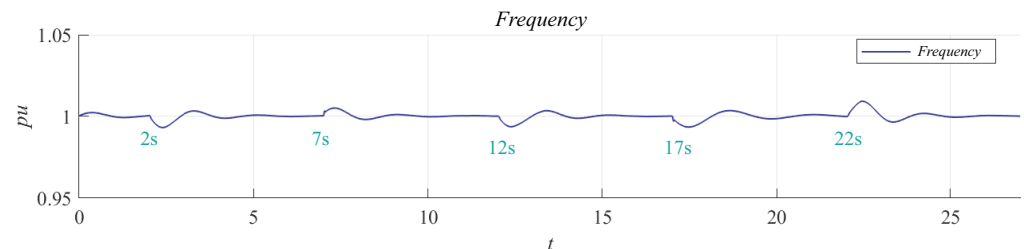


Figure 14. System frequency in per unit for case study 1.

The AVR regulates the system voltage for all the operation modes; Figure 15 shows the RMS voltage transients in the per unit system associated with the reactive power variations because of the changes in the wind power and loads.

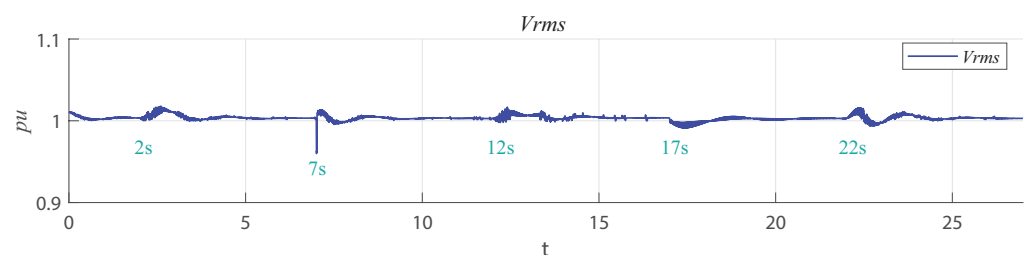


Figure 15. RMS voltage in per unit for case study 1.

5.2. Case Study 2

In this case study, the transition from WO mode to DO mode is shown. The power balance can be analysed as in the previous study case 1. In Figure 16, initially, the wind speed is high and the WTG provides an active power of 340 kW and 265 kW for a wind speed of 12 m/s and 11 m/s, respectively. In the period from $t = 15$ s to $t = 25$ s, there is no wind power production so the WDHS controller must promptly order engage the DG to the SM in order to produce the active power required by the consumer load.

The FESS and the DL are not absorbing active power, as shown in Figures 17 and 18, respectively, because there is no surplus of active power. The DG supplies the active power to the consumer load for low wind speed in DO mode, as illustrated in Figure 19. The DG generates the 85 kW required by the consumer load and after the consumer load changes to 35 kW, the DG also supplies that 35 kW properly.

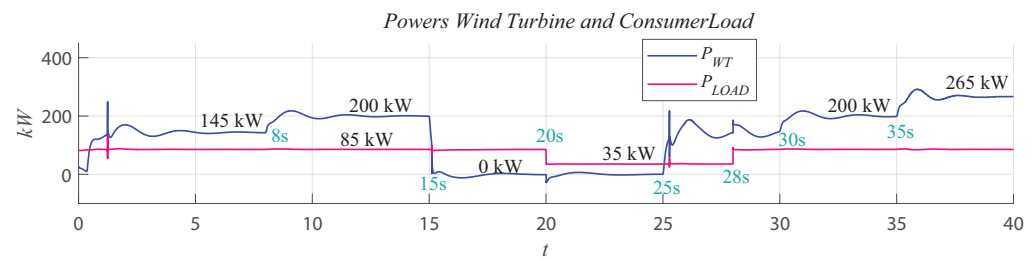


Figure 16. Power wind and load for case study 2.

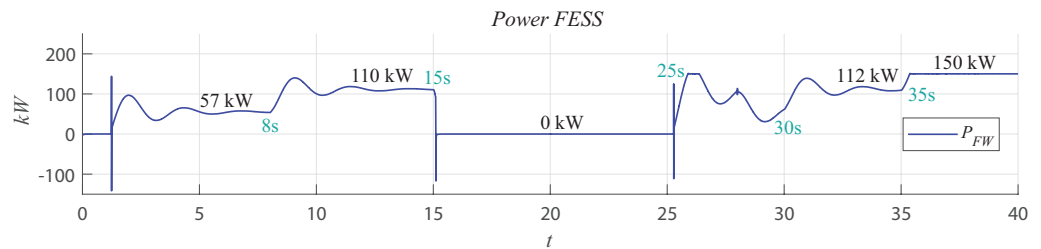


Figure 17. Power absorbed by the FESS for case study 2.

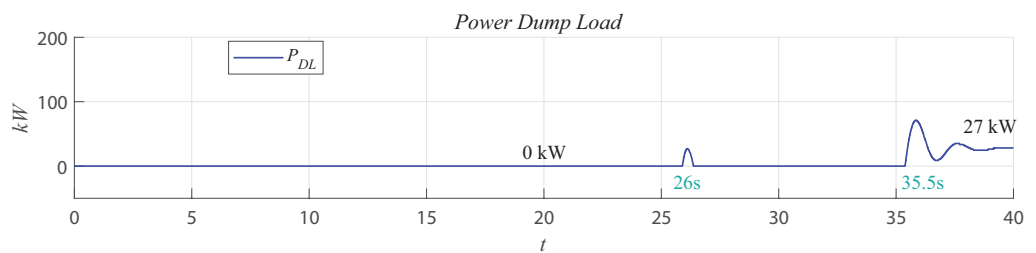


Figure 18. Power in the DL for case study 2.

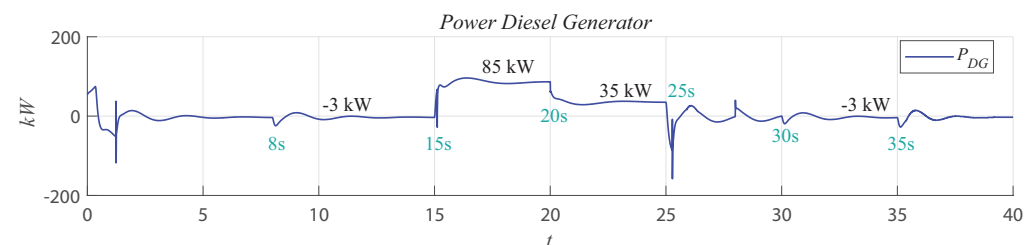


Figure 19. Power in the DG for case study 2.

The active power consumed by the DL is shown in Figure 18. As can be observed in this figure, the DL tries to consume a little active power in approximately 26 s. It is during this time, there is still excess active power and the FESS has reached its rated power and cannot store more power. This attempt to consume power lasts a short time (approx. 0.5 s) because once a transient has passed, the FESS still has the capacity to store active power. After that, in 35 s, an increase in active power produced by the wind turbine occurs, so after 35.5 s, once the FESS reaches its rated power, the DL starts to consume the active power excess because the FESS is fully charged during this time. The active power produced by the DG is shown in Figure 19.

At $t = 25$ s, the wind turbine starts producing power again sufficient to feed the consumer load, and a surplus of active power occurs. Therefore, the WDHS control must order to disengage the DG from the SM and change to WO mode. The power excess is absorbed by the FESS and the DL as shown in Figures 17 and 18, respectively. Moreover, in Figure 19, after $t = 25$ s, the SG stops producing active power because it works as a synchronous condenser and only consumes 3 kW corresponding to the mechanical losses.

Figure 20 shows the system frequency per unit for case study 2. Similar to case study 1, the frequency contains transients due to applied changes to wind speed and consumer load. As can be seen in this figure, the controller damps these frequency variations adequately.

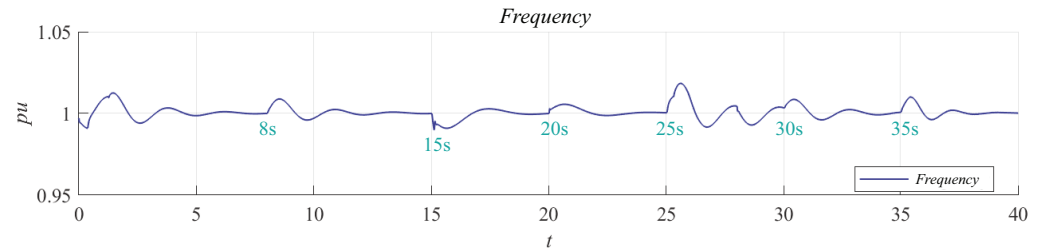


Figure 20. System frequency in per unit for case study 2.

The RMS voltage represented in the per unit system is shown in Figure 21. Similar to case 1, the voltage variations correspond to reactive power variations due to the changes applied in the WDHS and load. These variations are properly mitigated by the AVR.

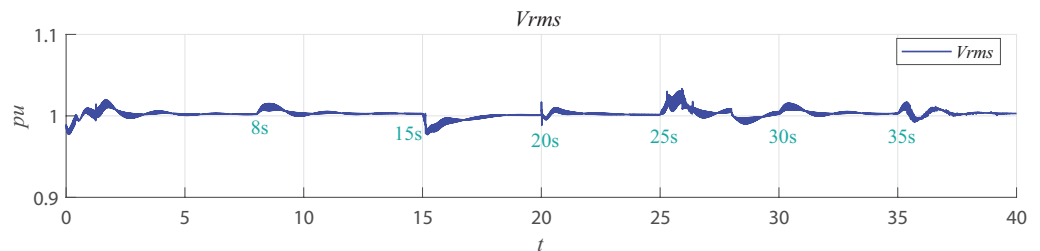


Figure 21. RMS voltage in per unit for case study 2.

5.3. Case Study 3

For this case study, the WDHS operates in DO mode at the beginning of the simulation and later the transition to WO operation mode is carried out. Figure 22 shows that, because there is no wind power, the WTG does not generate active power from $t = 0$ s to $t = 5$ s. Consequently, the DG supplies the active power needed by the consumer load in this period.

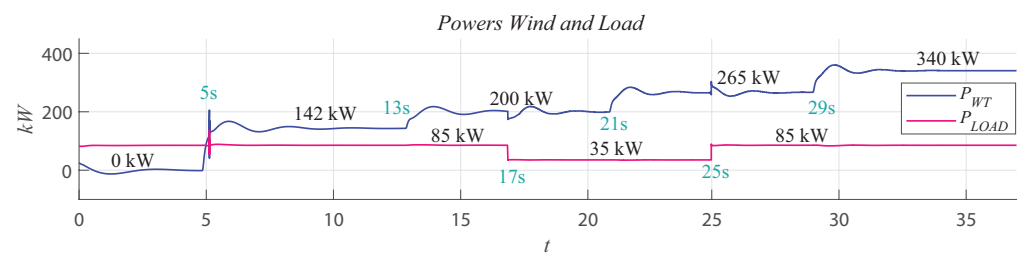


Figure 22. Power wind and load for case study 3.

Figures 23 and 24 show, respectively, that neither the FES nor the DL consumes active power since the wind turbine is not generating power. On the other hand, the DG supplies the total active power demanded by the consumer load, as can be seen in Figure 25. In Figure 22, the transition from DO to WO mode occurs at $t = 5$ s because the WTG starts to produce active power sufficient to feed the consumer load and the WDHS controller disengages the DG from the SM changing to WO. In this mode, the FESS consumes an active power of 54 kW from $t = 5$ s to $t = 13$ s, as shown in Figure 23, and in the same period, as shown in Figure 24, the DL does not consume power because the active power excess is lower than to full rating of the FESS.

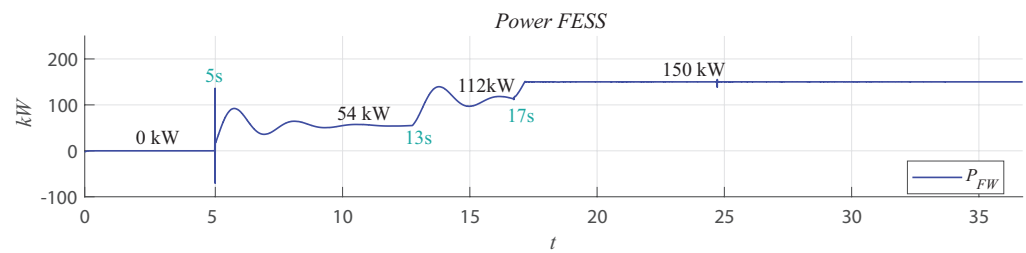


Figure 23. Power absorbed by the FESS for case study 3.

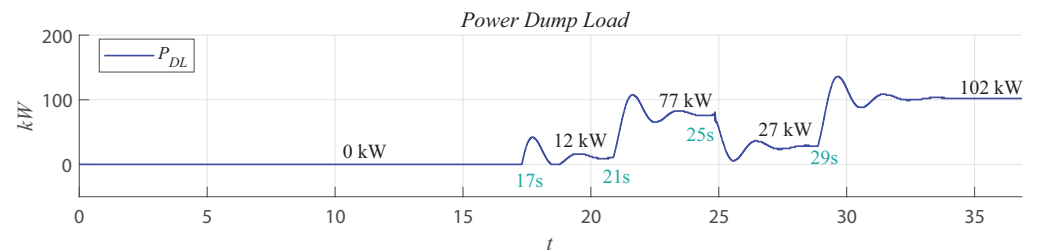


Figure 24. Power in the DL for case study 3.

The condition for the transition in the operation modes from WO to WD results from a frequency drop down to 59.4 Hz as a consequence of the wind power being lower than the consumer load. The condition for the transition from WD to WO is the result of a frequency increase up to 60.6 Hz as a consequence of power generation excess or in the case where the DG produces the minimum power recommended and dump loads are being actuated.

Because the power generated by the WTG continues increasing after $t = 5$ s, the FESS and the DL consumes the surplus of active power as shown in Figure 22. Specifically in the period from $t = 22$ s to $t = 25$ s, the WTG is generating 265 kW, the load consumption is 35 kW so that the power excess is 230 kW, which is consumed as follows: the FESS absorbs 150 kW, the DL consumes 77 kW and the DG consumes 3 kW accounting for the mechanical losses. For that period, these magnitudes can be seen in that period in Figures 23–25.

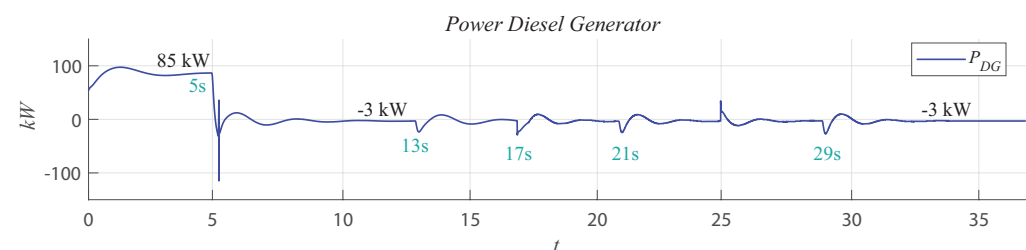


Figure 25. Power in the DG for case study 3.

Figures 26 and 27 show the system frequency and the RMS voltage in the per unit system, respectively, for case study 3. Similar to the previous cases studied, the variations are the results of changes applied to the system, and the controllers damp these variations properly.

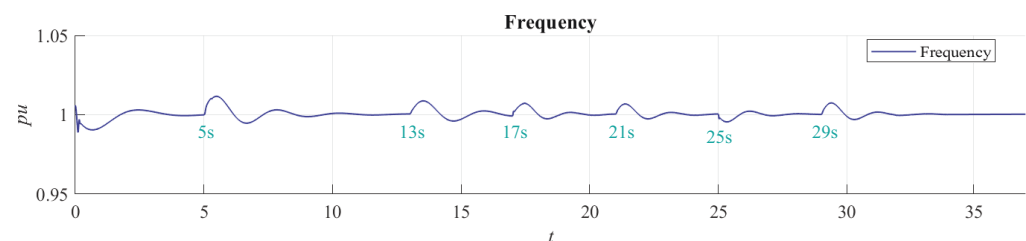


Figure 26. System frequency in per unit for case study 3.

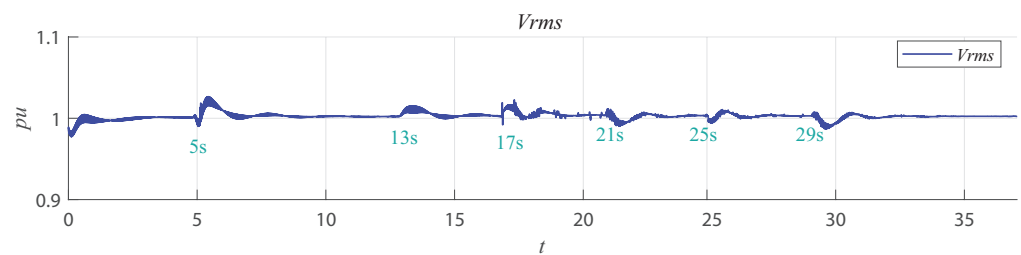


Figure 27. RMS voltage in per unit for case study 3.

6. Conclusions

Complete transitions of an HWDS were modelled and simulated in Matlab/Simulink. Each component along with its respective controller was described in detail, as well as the overall control of the HWDS. The FESS uses two three-phase full-bridge converters in a back-to-back configuration; the grid-side converter works as an interface between the FESS and the grid; the machine-side converter regulates the electrical torque in the FESS shaft. The FESS absorbs the wind power excess by accelerating the flywheel in periods of high wind speed. Conversely, the FESS supplies power to the consumer loads by decelerating the flywheel when the wind speed is low. The WDHS considered in this article uses a friction clutch to disengage the DE to the SG in WO mode. In WO operation mode, the synchronous generator works as a synchronous condenser. A PI controller properly tuned is used to control the system frequency by providing the power reference to the DL and the FESS. The proposed controller gives priority to the FESS over the DL in order to harness the wind resource. Simulation results show the correct function of the HP-WDPS during the different operation models with the proposed controllers maintaining the frequency and voltage within the proper limits for wind speed and load variations.

Author Contributions: All authors have made an important contribution to the creation of this paper. Conceptualization, J.L.M.-M. and R.P.-A.; methodology, J.L.M.-M., R.P.-A. and O.A.-L.; software, J.L.M.-M., R.P.-A. and D.C.-G.; validation, J.L.M.-M. and R.P.-A.; formal analysis, J.L.M.-M. and R.P.-A.; investigation, J.L.M.-M., R.P.-A., D.C.-G. and O.A.-L.; resources, J.L.M.-M. and R.P.-A.; data curation, J.L.M.-M. and R.P.-A.; writing—original draft preparation, J.L.M.-M., R.P.-A., D.C.-G. and O.A.-L.; writing—review and editing, J.L.M.-M., R.P.-A. and O.A.-L.; visualization, J.L.M.-M. and D.C.-G.; supervision, R.P.-A., D.C.-G. and O.A.-L.; project administration, R.P.-A., D.C.-G. and O.A.-L.; funding acquisition, D.C.-G. All authors have read and agreed to the published version of the manuscript.

Funding: This research received no external funding.

Conflicts of Interest: The authors declare no conflict of interest.

References

1. Ibrahim, H.; Dimitrova, M.H.; Dutil, Y.; Rousse, D.; Ilinca, A.; Perron, J. *Wind-Diesel Hybrid System: Energy Storage System Selection Method*; Academia: San Francisco, CA, USA, 2012.
2. Hunter, R.; Elliot, G. (Eds.) Designing a system. In *Wind-Diesel Systems: A Guide to the Technology and Its Implementation*; Cambridge University Press: Cambridge, UK, 1994; Chapter 4, pp. 95–138. [[CrossRef](#)]
3. Lu, C.; Xu, H.; Pan, X.; Song, J. Optimal Sizing and Control of Battery Energy Storage System for Peak Load Shaving. *Energies* **2014**, *7*, 8396–8410. [[CrossRef](#)]
4. Taj, T.A.; Hasanién, H.M.; Alolah, A.I.; Muyeen, S.M. Transient stability enhancement of a grid-connected wind farm using an adaptive neuro-fuzzy controlled-flywheel energy storage system. *IET Renew. Power Gener.* **2015**, *9*, 792–800. [[CrossRef](#)]
5. Suvire, G.; Mercado, P. Combined control of a distribution static synchronous compensator/flywheel energy storage system for wind energy applications. *IET Gener. Transm. Distrib.* **2012**, *6*, 483–492. [[CrossRef](#)]
6. El-Naga, A.A.; Marei, M.; El-Goharey, H. Second order adaptive notch filter based wind power smoothing using flywheel energy storage system. In Proceedings of the 2017 Nineteenth International Middle East Power Systems Conference (MEPCON), Cairo, Egypt, 19–21 December 2017; pp. 314–319.
7. Bai, L.; Li, F.; Hu, Q.; Cui, H.; Fang, X. Application of battery-supercapacitor energy storage system for smoothing wind power output: An optimal coordinated control strategy. In Proceedings of the 2016 IEEE Power and Energy Society General Meeting (PESGM), Boston, MA, USA, 17–21 July 2016; pp. 1–5.

8. Pathomchaiwat, P.; Neammanee, B. Control of power management in the renewable energy system by using Flywheel Energy Storage. In Proceedings of the 2017 14th International Conference on Electrical Engineering/Electronics, Computer, Telecommunications and Information Technology (ECTI-CON), Phuket, Thailand, 27–30 June 2017; pp. 513–516.
9. Wei, K.; Dai, X.; Liu, P. Model and balance of flywheel energy storage system with composite flywheel and rolling bearings. In Proceedings of the 2017 IEEE Conference on Energy Internet and Energy System Integration (EI2), Beijing, China, 26–28 November 2017; pp. 1–6.
10. Liu, Y.; Shi, L.; Zhao, L.; Li, Y. The controls of motors in flywheel energy storage system. In Proceedings of the 2014 9th IEEE Conference on Industrial Electronics and Applications, Hangzhou, China, 9–11 June 2014; pp. 179–182.
11. Xingjian, D.; Kunpeng, W.; Xiaozhang, Z.; Xinjian, J.; Kai, Z. A review on flywheel energy storage technology in fifty years. *Energy Storage Sci. Technol.* **2018**, *7*, 765.
12. Dai, X. Review on advanced flywheel energy storage system with large scale. *Diangong Jishu Xuebao (Trans. China Electrotech. Soc.)* **2011**, *26*, 133–140.
13. Cimuca, G.; Breban, S.; Radulescu, M.M.; Saudemont, C.; Robyns, B. Design and control strategies of an induction-machine-based flywheel energy storage system associated to a variable-speed wind generator. *IEEE Trans. Energy Convers.* **2010**, *25*, 526–534. [[CrossRef](#)]
14. Gayathri, N.S.; Senroy, N.; Kar, I.N. Smoothing of wind power using flywheel energy storage system. *IET Renew. Power Gener.* **2017**, *11*, 289–298. [[CrossRef](#)]
15. Díaz-González, F.; Sumper, A.; Gomis-Bellmunt, O. *Energy Storage in Power Systems*; John Wiley & Sons: Hoboken, NJ, USA, 2016.
16. Karrari, S.; Noe, M.; Geisbuesch, J. High-speed flywheel energy storage system (FESS) for voltage and frequency support in low voltage distribution networks. In Proceedings of the 2018 IEEE 3rd International Conference on Intelligent Energy and Power Systems (IEPS), Kharkiv, Ukraine, 10–14 September 2018; pp. 176–182.
17. Villanueva, I.; Torres, E.; Balderas, D.; Ponce, P.; Molina, A. Supervisory Controller for Smoothing Wind Turbine Power Output based on FESS using ANNs for Short-Term Ahead Prediction. In Proceedings of the IECON 2018—44th Annual Conference of the IEEE Industrial Electronics Society, Washington, DC, USA, 21–23 October 2018; pp. 1964–1969.
18. Zhou, L.; Tang, X.; Qi, Z. Control method for flywheel array energy storage system in energy harvesting from electric railway. In Proceedings of the 2014 IEEE Conference and Expo Transportation Electrification Asia-Pacific (ITEC Asia-Pacific), Beijing, China, 31 August–3 September 2014; pp. 1–5.
19. Xiaojing, S.; Xinggui, W.; Haitao, Z.; Chunling, W. Research on Charge Control of New UPS Based on Flywheel Battery. *Int. J. Digit. Content Technol. Appl.* **2013**, *7*, 770.
20. Aitchison, D.R.; Cirrincione, M.; Leijtens, N. Design development of a flywheel energy storage system for isolated pacific island communities. In Proceedings of the 2016 IEEE international conference on advanced intelligent mechatronics (AIM), Banff, AB, Canada, 12–15 July 2016; pp. 1628–1633.
21. Ažubalis, M.; Baranauskas, A.; Tamulis, G. Wind power balancing using flywheel energy storage system. *Elektron. Elektrotech.* **2013**, *19*, 19–22. [[CrossRef](#)]
22. Gurumurthy, S.R.; Agarwal, V.; Sharma, A. Optimal energy harvesting from a high-speed brushless DC generator-based flywheel energy storage system. *IET Electr. Power Appl.* **2013**, *7*, 693–700. [[CrossRef](#)]
23. Gonçalves de Oliveira, J. Power Control Systems in a Flywheel Based All-Electric Driveline. Ph.D. Thesis, Acta Universitatis Upsaliensis, Uppsala, Sweden, 2011.
24. Lone, S.A.; Mufti, M.U.D. Power quality improvement of a stand-alone power system subjected to various disturbances. *J. Power Sources* **2006**, *163*, 604–615. [[CrossRef](#)]
25. Papathanassiou, S.A.; Papadopoulos, M.P. Dynamic characteristics of autonomous wind–diesel systems. *Renew. Energy* **2001**, *23*, 293–311. [[CrossRef](#)]
26. Muljadi, E.; Mckenna, H.E. Power quality issues in a hybrid power system. *IEEE Trans. Ind. Appl.* **2002**, *38*, 803–809. [[CrossRef](#)]
27. Carrillo, C.; Feijóo, A.; Cidrás, J. Comparative study of flywheel systems in an isolated wind plant. *Renew. Energy* **2009**, *34*, 890–898. [[CrossRef](#)]
28. Jia, Y.; Wu, Z.; Zhang, J.; Yang, P.; Zhang, Z. Control Strategy of Flywheel Energy Storage System Based on Primary Frequency Modulation of Wind Power. *Energies* **2022**, *15*, 1850. [[CrossRef](#)]
29. Amiryar, M.E.; Pullen, K.R. Assessment of the carbon and cost savings of a combined diesel generator, solar photovoltaic, and flywheel energy storage islanded grid system. *Energies* **2019**, *12*, 3356. [[CrossRef](#)]
30. Hansen, A.D.; Iov, F.; Sørensen, P.; Cutululis, N.; Jauch, C.; Blaabjerg, F. *Dynamic Wind Turbine Models in Power System Simulation Tool DIgSILENT*; U.S. Department of Energy Office of Scientific and Technical Information: Oak Ridge, TN, USA, 2007.
31. Margaritis, I.D.; Papathanassiou, S.A.; Hatziaargyriou, N.D.; Hansen, A.D.; Sorensen, P. Frequency control in autonomous power systems with high wind power penetration. *IEEE Trans. Sustain. Energy* **2012**, *3*, 189–199. [[CrossRef](#)]
32. Beyer, H.; Degner, T.; Gabler, H. Operational behaviour of wind diesel systems incorporating short-term storage: An analysis via simulation calculations. *Sol. Energy* **1995**, *54*, 429–439. [[CrossRef](#)]
33. Sebastián, R.; Alzola, R.P. Flywheel energy storage systems: Review and simulation for an isolated wind power system. *Renew. Sustain. Energy Rev.* **2012**, *16*, 6803–6813. [[CrossRef](#)]
34. Harnefors, L.; Nee, H.P. A general algorithm for speed and position estimation of AC motors. *IEEE Trans. Ind. Electron.* **2000**, *47*, 77–83. [[CrossRef](#)]

-
35. Umland, J.W.; Safiuddin, M. Magnitude and symmetric optimum criterion for the design of linear control systems: What is it and how does it compare with the others? *IEEE Trans. Ind. Appl.* **1990**, *26*, 489–497. [[CrossRef](#)]
 36. Leonhard, W. *Control of Electrical Drives*; Springer Science & Business Media: Berlin/Heidelberg, Germany, 2001.